A&A 488, L75–L78 (2008)
DOI: 10.1051/0004-6361:200810462

Astronomy & Astrophysics

Letter to the Editor

VLT/NACO and Subaru/CIAO *JHK*-band high-resolution imaging polarimetry of the Herbig Be star R Monocerotis

K. Murakawa[1], T. Preibisch[1], S. Kraus[1], N. Ageorges[2], K.-H. Hofmann[1], M. Ishii[3], S. Oya[3], A. Rosen[1], D. Schertl[1], and G. Weigelt[1]

[1] Max-Planck-Institut für Radioastronomie, Auf dem Hügel 69, 53121 Bonn, Germany
e-mail: murakawa@mpifr-bonn.mpg.de
[2] European Southern Observatory (ESO), Alonso de Cordova 3107, Vitacura, Casilla 19001, Santiago 19, Chile
[3] Subaru Telescope, National Astronomical Observatory of Japan, 650 North A'ohoku place, Hilo, HI 96720, USA

Received 25 June 2008 / Accepted 30 July 2008

ABSTRACT

Aims. We investigate the dust properties of the disk and envelope of the Herbig Be star R Mon by means of near-infrared multiwavelength imaging polarimetry.
Methods. We obtained JHK-band polarimetric images using the adaptive optics instruments NACO on the VLT, and CIAO on the Subaru telescope.
Results. Our NACO JK_S-band images of ~0.″1 angular resolution resolve clearly the R Mon binary system as well as twisted string-like features in the fan-shaped lobe. The polarimetric images reveal a butterfly-shaped polarization disk with an almost constant shape and an extension of 4″ in the J, H, and K bands. In this region, the polarization values are as low as $P_J \sim 7\%$, $P_H \sim 2\%$, and $P_K \sim 1\%$, and the polarization vectors are not systematically aligned along the equatorial plane. On the other hand, highly polarized scattered light is detected in the fan-shaped lobe ($P_J \sim 24\%$, $P_H \sim 33\%$, and $P_K \sim 53\%$).
Conclusions. Our polarimetric data suggests the presence of multiple grain populations in the R Mon nebula. From our one-dimensional single scattering modeling, the maximum grain size in the nebula at large scale is estimated to be 0.23 μm. On the other hand, the aforementioned properties of the polarization disk and a nearly spherical appearance of the nebulosity close to the central star suggests the presence of large grains (micron-size or larger) in the polarization disk.

Key words. stars: individual: R Monocerotis – circumstellar matter – stars: imaging – ISM: reflection nebulae – infrared: stars

1. Introduction

R Mon is located at a distance of ~800 pc (Jones & Herbig 1982) and is classified as a Herbig Be star (Herbig 1960) of a spectral type of B0 (Hillenbrand et al. 1992) and a luminosity of ~1400 $L_\odot$ (Cohen et al. 1984). This star illuminates the fan-shaped reflection nebula NGC 2261, which is also known as Hubble's variable nebula. The appearance of this nebula varies on timescales of months and years (e.g. Lightfoot 1989; Scarrott et al. 1989). Radio observation discovered a bipolar CO outflow with a northern blue-shifted and a southern red-shifted component (Cantó et al. 1981). The northern lobe is clearly dominant and is tilted towards the observer (Walsh & Malin 1985).

Imaging and imaging polarimetry of sub-arcsec resolution revealed several dusty structures in the vicinity of R Mon. Close et al. (1997) obtained JHK'-band intensity images and H-band polarimetric images of a 0.″2 resolution using the 19-element University of Hawaii adaptive optics (AO) of the 3.6 m CFH telescope, and also used an HST optical image to analyze the circumstellar envelope of R Mon. They discovered the T Tauri companion R Mon B with a 0.″69 separation. Furthermore, their polarimetric data revealed a polarization disk extending in the east-west direction, bisecting the nebula and implied that an optically thick dust structure was present around the central star. Weigelt et al. (2002) presented H- and K-band diffraction-limited bispectrum speckle interferometry of 55 mas, for H band, and 76 mas, for K band resolutions and detected a bright arc-shaped structure pointing away from R Mon in the north-western direction. They interpreted this feature as the surface of a dense structure close to the thick circumstellar disk or torus around R Mon.

Dust is a key component of the disk and envelope around young stellar objects (YSOs). Near-infrared imaging polarimetry is a powerful technique to probe such a dusty environment (e.g. Bastien & Ménard 1988; Kenyon et al. 1993; Whitney et al. 1997). We performed high-resolution imaging polarimetry of R Mon in the JHK-bands using AO-equipped 8 m telescopes to investigate the grain properties of the nebula.

2. Observations and results

2.1. NACO J-band imaging and K_S-band polarimetry

We obtained J-band standard (non-polarimetric) images and K_S-band polarimetric images using the CONICA camera and the NAOS AO system with its 185-element Shack-Hartmann sensor on the VLT. The observations were carried out on November 1, 2006 and December 22, 2006. We used the S13 camera with a pixel scale of 13.27 mas pix^{-1}. The natural seeing varied between 0.″7 and 1.″2 for the J-band imaging, and 0.″5 and 0.″6 for the K_S-band polarimetry. We adopted the N20C80 dichroic filter for the NAOS wavefront sensing and on-source AO wavefront sensing. For the K_S-band polarimetry, we used the turnable half-waveplate (HWP) and the fixed wire grid polarizer. To measure

linear polarization, we obtained four image sets with position angles of the HWP of 0°, 45°, 22.5°, and 67.5°. For the K-band polarimetry, the total integration time was 21 min. We used the K_S-band polarimetric data of the reflection nebula Frosty Leo for polarization calibration and found that the polarization maps obtained from our NACO observations agree with those of the CIAO maps. In the J band, we obtained images with a total integration time of 8 min, applying four jitter offset positions. For the flux calibration, we observed the photometric standard stars of GSPC S824-E in the J band and GSPC S372-S in the K_S band. We measured signal-to-noise ratio values of 10–30 per pixel for the J-band intensity image and 30–100 for the K_S-band Stokes I images. The error of linear polarization was lower than 2% per pixel. The measured PSF sizes were 0.″11 in the J band and 0.″066 in the K_S band.

2.2. CIAO imaging polarimetry in the JHK bands

We obtained JHK-band polarimetric images using the CIAO instrument and AO with the 36-element curvature sensor on the 8 m Subaru telescope. The data were recorded on December 28, 2006 using the medium-resolution camera with a pixel scale of 21.7 mas pix^{-1}. The natural seeing was ∼1.″5 in the R band during observations. Since R Mon is sufficiently bright (m_R = 11.8 mag) in the R band (the wavelength for wavefront sensing) and there is no bright single star close to R Mon, we applied on-source AO wavefront sensing. We followed the observation sequence described in our previous paper (Murakawa et al. 2005). The total integration times were 18 min, 16 min, and 20 min for the J, H, and K bands, respectively. We also observed NGC 1333 #5 to enable us to complete a polarization calibration. The data reduction was completed as described in our previous papers (Murakawa et al. 2004, 2005). After subtraction of the dark frames and flat-fielding, we obtained images of the Stokes IQU, the degree of polarization (P), and the polarization position angle (θ), as well as their error images. We found signal-to-noise ratios of 30–100 per pixel for the Stokes I images. The error of linear polarization was lower than 2% for the J and H bands and lower than 4% for the K band. The measured PSF sizes were 0.″54 in the J band and 0.″35 in the H and K bands, reflecting the poor sky conditions[1]. In previous observations with the AO, the measured PSF sizes typically achieved were ∼0.″1, in natural seeing of higher quality than 0.″7, in the R band (Oya et al. 2004).

2.3. Results

Figure 1 presents the results of our NACO and CIAO observations. All intensity images show the well-known fan-shaped nebulosity extending towards the north, the prominent central star feature, and a string-like feature extending ∼2″ towards the northeast. The high angular resolution of our NACO images resolve the string-like feature and the binary companion R Mon B. The central star feature looks almost spherical in the K band but slightly triangular in the J band. In addition, we confirm an arc-shaped feature extending from the central star towards the northwest, which was discovered in previous speckle images (Weigelt et al. 2002). Our CIAO images resolved a handle-like feature extending 5″ towards the southeast. This feature is also seen in the previous images by Close et al. (1997), but appears in the southwest direction on a large scale of ∼100″ in the R-band image (Warren-Smith et al. 1987).

Our polarimetric data confirms a centro-symmetric polarization vector pattern surrounding the central star in the nebula, a polarization disk, and polarization null points along the polarization disk, which were already presented in previous papers (e.g., Close et al. 1997). Our multiple-band data revealed some more interesting results. Our data resolve sufficiently the polarization disk, which has a 4″ extension in east-west with $P < 10\%$. Its size alters little between the J, H, and K bands. Polarization vectors in this region are often aligned almost along the polarization disk in several young stars, but this is not obvious in R Mon. Along the arc-shaped feature, the degree of polarization is higher than in the surrounding region at distances of up to ∼0.″4 in all bands. The polarization vectors there are aligned approximately perpendicularly to the arc, providing evidence that the arc is being observed in singly scattered light. We, therefore, interpret this arc as the western wall of an outflow or a disk surface.

To investigate the wavelength dependence of the polarization, we performed aperture polarimetry at several interesting regions. Table 1 summarizes the measured degree of polarization and polarization orientation at the central star (A), the string-feature (B), the northwest rim of the nebulosity (C), and the arc-like feature (D). While highly polarized fluxes are detected at the string-like feature and the northwest rim ($P_J \sim 24\%$, $P_H \sim 33\%$, and $P_K \sim 53\%$ at C), the polarization towards the central star (A) decreases with increasing wavelength. At the 0.″1 aperture, the J band polarization ($P_J = 7\%$) becomes abruptly higher than in the H and K bands ($P_H = 1.5\%$ and $P_K = 1.1\%$). At larger apertures, the polarization varies more gradually and the polarization orientations become closer to those at position B. This is due to contamination by the polarized flux from the string-like feature. It is also interesting to compare the above results to other YSOs. For massive YSOs, high polarizations ($P \sim 20\%$ at K) are often detected (e.g. CRL 2136, AFGL 2591, and Ori BN observed by Hough et al. 1989; and Holloway et al. 2002). In these objects, polarization vectors close to the central star are aligned nearly along the polarization disk, e.g. CRL 2136, (Murakawa et al. 2008a), AFGL 2591, (Minchin et al. 1991b). These high polarizations and the polarization vector alignment are probably due to dichroic extinction by small non-spherical grains (Serkowski et al. 1975; Hough et al. 1989; Murakawa et al. 2008a). On the other hand, low polarizations (e.g. $P \sim 1\%$ at K) are observed in T Tauri stars (Bastien 1985; Whittet et al. 1992; Kobayashi et al. 1999). Ménard et al. (1988) argued that a low polarization is produced by light scattered from comparably large grains ($a \gtrsim \lambda$) close to the central star rather than a cancellation of the polarized component by summing the randomly oriented polarized scattered light by a large aperture. Near-infrared high-resolution polarimetric images of a low mass proto-stellar object HL Tau, in fact, show almost zero polarization in the vicinity of the central star and no systematically aligned polarization pattern (Lucas et al. 2004; Murakawa et al. 2008b). The properties of the polarization disk of R Mon are more similar to low mass YSOs than massive stars.

3. Discussion

The high polarization in the nebula suggests that submicron-size grains exist in this region. We have estimated their size by means of a single scattering polarization analysis with a one-dimensional spherical dust shell model (Dougados et al. 1990). When using the polarization data measured at the rim of the fan-shaped nebula, this simple analysis provided a rough estimate

[1] Because of a different sky condition between our CIAO and NACO observations, it is meaningless to directly compare the performance of the Subaru AO and the NAOS from our data.

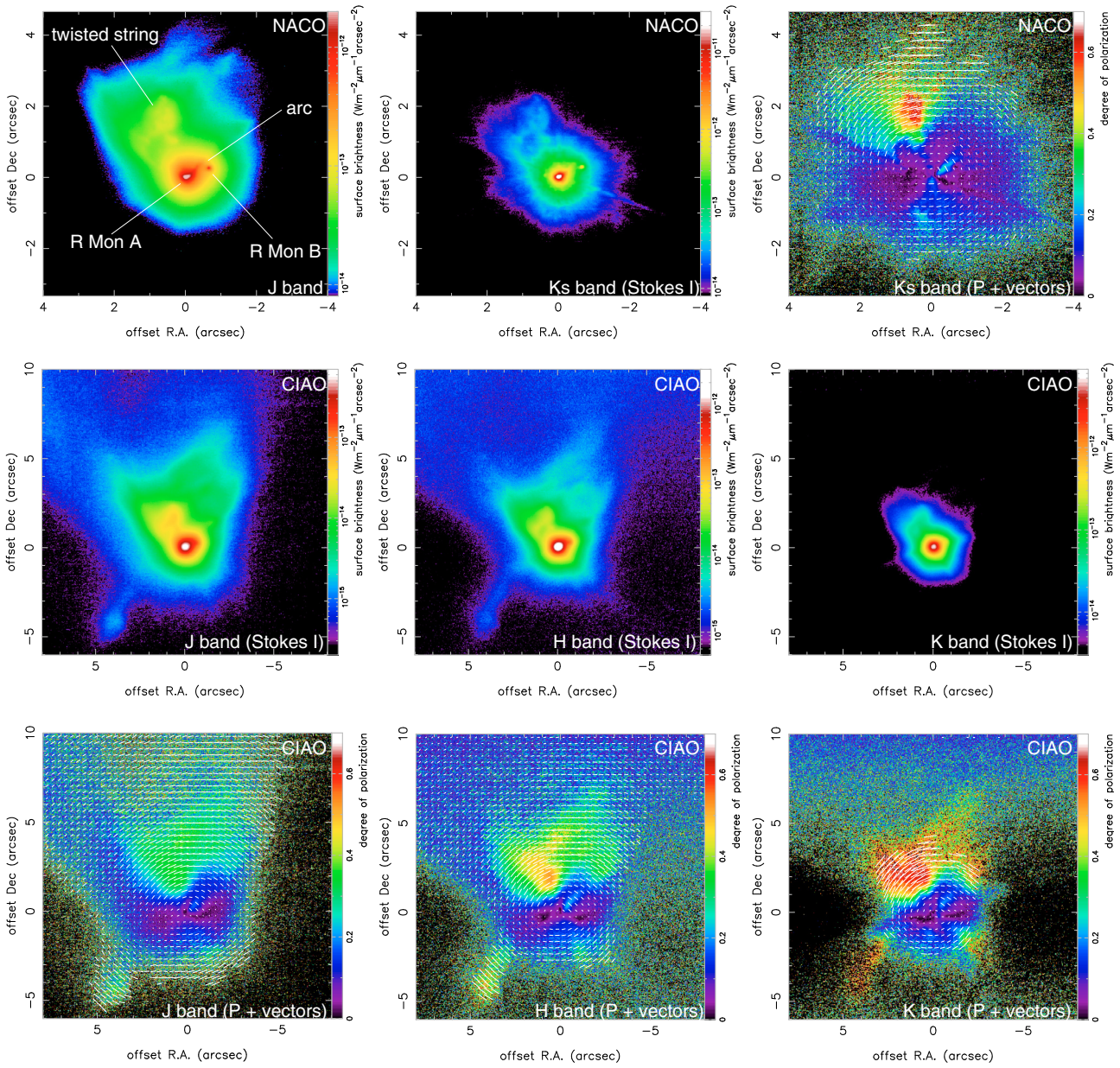

Fig. 1. JHK-band polarimetric data of R Mon. The top panels show the VLT/NACO J- and K_S-band intensity images and the degree of polarization image (P) overlaid with the polarization vector lines (i.e., degree of polarization and position angle of the electric field). The field of view (FOV) is $8'' \times 8''$. In the K_S-band image, spike-like features seen at position angles of 69° and −111° are diffraction patterns of the supporter of the telescope secondary mirror. *The middle and bottom panels* show the Stokes I images and the degree of polarization images (P) in the JHK bands, respectively, which were obtained using the Subaru/CIAO. The FOV is $16'' \times 16''$. The polarization vector lines are also drawn on the degree of polarization images. In all images, north is up and east to the left. The position of the central star is indicated by the offset position of (0.″0, 0.″0).

Table 1. Results of aperture polarimetry based on our CIAO data.

Location	P_J (%)	θ_J (°)	P_H (%)	θ_H (°)	P_K (%)	θ_K (°)
A1 (aperture = 0.″1)	7.1	48.5	1.5	4.0	1.1	−75.7
A2 (aperture = 2″)	4.3	22.3	4.0	21.2	3.3	−4.7
A3 (aperture = 5″)	5.5	−8.5	4.2	−5.3	3.8	−9.2
B (offset = (0.″66, 1.″73), PA = 21°)	34.7	−23.0	50.7	−24.8	60.4	−27.4
C (offset = (−2.″25, 2.″48), PA = −42°)	24.0	35.9	32.7	36.0	53.0	33.9
D (offset = (−0.″36, 0.″25), PA = −55°)	16.8	45.5	21.3	44.6	16.6	37.0

The P and θ denote the degree of polarization and polarization position angle, respectively. The subscripts indicate the values for the J, H, or K band. A1, A2, and A3: at the central star. B: at the string-like feature. C: at the northwestern lobe. D: at the arc-like feature. A 0.″3 diameter aperture is applied for the B, C, and D measurements. The values in the brackets at B, C, and D denote the offset position and the PAs with respect to the central star (A).

of the grain size (see Murakawa et al. 2008a), which does not depend strongly on the geometrical parameters. Applying an inner radius $R_{\rm in}$ = 1 AU (Fuente et al. 2006), an outer radius $R_{\rm out}$ = 20 000 AU, a radial dust density distribution $\rho \propto R^{-1.5}$, and a DL-MRN grain model (Mathis et al. 1977; Draine & Lee 1984) with a minimum size of 0.005 μm and a power-law size distribution $n(a) \propto a^{-3.5}$, we obtained a maximum grain size of 0.23 μm, which explains our JHK-band polarizations at location C well. This value is typical of interstellar grains. In contrast, we did not find a good solution to reproduce the polarization values at the string-like feature (location B). A higher polarization of this feature is probably due to a geometrical effect, that is this feature is orientated roughly along the plane of sky, as argued by Minchin et al. (1991a).

On the other hand, the grain properties close to the central star are very different. Fuente et al. (2006) presented high-resolution images of R Mon in the 1.3 mm and 2.7 mm dust continua. They regarded a 0.″3 (120 AU) extension at 1.3 mm as a disk. This compact feature is the only flux source that causes the flux excess at millimeter wavelengths, where an opacity index β (Beckwith & Sargent 1991) is found to be 0.3–0.5 (Fuente et al. 2003, 2006). From their result, this disk is expected to be a region filled with large grains of the order of millimeter size. The presence of large grains is also expected from our data, as described in the previous section. Furthermore, a Keplerian rotating motion was detected with a 2″ (1500 AU) radius in the ^{12}CO emission line data (Fuente et al. 2006). Interestingly, this size is in good agreement with the angular size of the polarization disk detected in our images. Taking into account that rotating motion is an important factor for grain growth, that the size and appearance of the polarization disk are almost identification in the J, H, and K bands, and that an equatorial waist due to the thick disk is not clearly detected around the central star, it is possible that grains that have grown micron-size exist in the region within 1500 AU.

The mechanisms to produce polarization and depart from a centro-symmetric polarization vector pattern in the polarization disk have been discussed and still remain controversial topics. Possible explanations include: (1) dichroic extinction by aligned non-spherical grains (e.g. Mestel & Paris 1984) and (2) multiple-scattering in the disk (Bastien & Ménard 1988). Ménard et al. (1988), hereafter MBR88, obtained a circular polarization image of R Mon and NGC 2261 in the optical to determine which explanation is more likely for this object. They pointed out that the magnetic field structure is uncertain and is expected to be very complex in the circumstellar environment, suggesting that it is difficult to explain both the circular and linear polarization. Furthermore, the multiple-epoch data shows that the orientations of the polarization disk and the vector alignment changed in a few years (Scarrott et al. 1989). Such a rapid temporal variation can be explained with the moving shadow effect, i.e. the motion of the illuminated regions in the nebula, but not with the grain alignment. However, this latter effect leaves the grain properties in the disk. BMR88 proposed an alternative model of multiple scattering in R Mon. This model requires only spherical grains and a geometrically thin, optically thick disk, and aligned polarization vectors can be explained in many YSOs (Bastien & Ménard 1988, 1990). If a disk structure is resolved sufficiently, a polarization enhancement and aligned polarization vectors along the polarization disk at the disk boundary are expected to appear in the polarization images, according to their model. However, we do not find explicit evidence in our data. The arc-like feature probably appears due to scattering, but the polarized flux is produced by single scattering, as discussed in Sect. 2.3. The polarization vector alignment in the polarization disk detected in previous data (e.g. Warren-Smith et al. 1987; Scarrott et al. 1989) is produced with scattered light mainly from the northern nebula due to an extended PSF side lobe rather than multiple scattering. There are two possible explanations of the negative detection of evidence for multiple scattering. The first explanation is that the disk is filled with large grains (micron-size or larger). The models presented by Bastien & Ménard (1988) used small grains ($a \sim 0.2$ μm). However, multiple scattering by large grains does not produce a high polarization. The second possible explanation is that the disk does not have a geometrically thin structure. If the disk is puffed up and the disk boundary is located close to the polar region, the polarization vectors are aligned perpendicularly to the disk or centro-symmetrically, even if only small grains exist in the disk. Such a result was reported for CRL 2136 (Murakawa et al. 2008a). For R Mon, a high value of the disk scale height of 1 is estimated from the CO emission line image (Fuente et al. 2006). If the dust disk also has such a geometrically thick structure without an advanced dust settlement, the polarization vector alignment is unlikely to be present.

Our high-resolution polarimetric data revealed the detailed structure of the polarization disk. This provides useful information about grain properties that is difficult to derive from low-resolution data. Further analysis, which takes into account non-spherical grains and geometrically thin disks will clarify which models, i.e. the aligned grains or multiple scattering, are more likely in R Mon.

References

Bastien, P. 1985, ApJS, 59, 277
Bastien, P., & Ménard, F. 1988, ApJ, 326, 334
Bastien, P., & Ménard, F. 1990, ApJ, 364, 232
Beckwith, S. V. W., & Sargent, A. I. 1991, ApJ, 381, 250
Cantó, J., Rodriguez, L. F., Barral, J. F., & Carral, P. 1981, ApJ, 244, 102
Close, L. M., Roddier, F., Hora, J. L., et al. 1997, ApJ, 489, 210
Cohen, M., Harvey, P. M., Wilking, B. A., et al. 1984, ApJ, 278, 671
Dougados, C., Rouan, D., Lacombe, F., et al. 1990, A&A, 227, 437
Draine, B. T., & Lee, H. M. 1984, ApJ, 285, 89
Fuente, A., Rodríguez-Franco, A., Testi, L., et al. 2003, ApJ, 598, L39
Fuente, A., Alonso-Albi, T., Bachiller, et al. 2006, ApJ, 649, L119
Herbig, G. H. 1960, ApJS, 4, 337
Hillenbrand, L. A., Strom, S. E., Vrba, F. J., & Keene, J. 1992, ApJ, 397, 613
Holloway, R. P., Chrysostomou, A., Aitken, D. K., Hough, J. H., & McCall, A. 2002, MNRAS, 336, 425
Hough, J. H., Whittet, D. C. B., Sato, S., et al. 1989, MNRAS, 241, 71
Jones, B. F., & Herbig, G. H. 1982, AJ, 87, 1223
Kenyon, S. J., Whitney, B. A., Gomez, M., & Hartmann, L. 1993, ApJ, 414, 773
Kobayashi, N., Nagata, T., Tamura, M., et al. 1999, ApJ, 517, 256
Lightfoot, J. F. 1989, MNRAS, 239, 665
Lucas, P. W., Fukagawa, M., Tamura, M., et al. 2004, MNRAS, 352, 1347
Mathis, J. S., Rumple, W., & Nordsieck, K. H. 1977, ApJ, 217, 425
Ménard, F., Bastien, P., & Robert, C. 1988, ApJ, 335, 290 (MBP88)
Mestel, L., & Paris, R. B. 1984, A&A, 136, 98
Minchin, N. R., Hough, J. H., McCall, A., et al. 1991a, MNRAS, 249, 707
Minchin, N. R., Hough, J. H., McCall, A., et al. 1991b, MNRAS, 251, 508
Murakawa, K., Suto, H., Tamura, M., et al. 2004, PASJ, 56, 509
Murakawa, K., Suto, H., Oya, S., et al. 2005, A&A, 436, 601
Murakawa, K., Preibisch, T., Kraus, S., & Weigelt, G. 2008a, A&A, accepted
Murakawa, K., Oya, S., Pyo. T.-S., & Ishii, M. 2008b, A&A, submitted
Oya, S., Takato, N., Takami, H., et al. 2004, Proc. SPIE, 5490, 409
Scarrott, S. M., Draper, P. W., & Warren-Smith, R. F. 1989, MNRAS, 237, 621
Serkowski, K., Mathewson, D. S., & Ford, V. L. 1975, ApJ, 196, 261
Walsh, J. R., & Malin, D. F. 1985, MNRAS, 217, 31
Warren-Smith, R. F., Draper, P. W., & Scarrott, S. M. 1987, ApJ, 315, 500
Weigelt, G., Balega, Y. Y., Hofmann, K.-H., & Preibisch, T. 2002, A&A, 392, 937
Whitney, B. A., Kenyon, S. L., & Gomez, M. 1997, ApJ, 485, 703
Whittet, D. C. B., Martin, P. G., Hough, J. H., et al. 1992, ApJ, 386, 562